

**BIFURCATION OF A SQUARE PLATE
TWISTED BY CORNER FORCES**

By

Raymon Miya

B.A.Sc. (Mechanical Engineering), University of Waterloo, 1992

A THESIS SUBMITTED IN PARTIAL FULFILLMENT OF
THE REQUIREMENTS FOR THE DEGREE OF
MASTER OF APPLIED SCIENCE

in

THE FACULTY OF GRADUATE STUDIES
DEPARTMENT OF MECHANICAL ENGINEERING

We accept this thesis as conforming
to the required standard

THE UNIVERSITY OF BRITISH COLUMBIA

April 1994

© Raymon Miya, 1994

In presenting this thesis in partial fulfilment of the requirements for an advanced degree at the University of British Columbia, I agree that the Library shall make it freely available for reference and study. I further agree that permission for extensive copying of this thesis for scholarly purposes may be granted by the head of my department or by his or her representatives. It is understood that copying or publication of this thesis for financial gain shall not be allowed without my written permission.

(Signature)

Department of Mechanical Engineering

The University of British Columbia
Vancouver, Canada

Date 25 April 1994

Abstract

A square plate twisted by corner forces is described by classical linear theory as a saddle surface. In an experiment, as the plate deforms to any noticeable deflection, it appears not as a saddle surface, but as a cylindrical surface. The transformation in mode shapes presents problems in determining material behaviour by shear in a plate twisting experiment. The two mode shapes can be described by either displacement or curvature of the surface. The purpose of this work is to investigate the buckling of a square plate twisted by corner forces by determining the bifurcation point and comparing the present FEA work with the experimental results of Howell and other results found in literature. The problem is examined using nonlinear finite element buckling analysis. The bifurcation point is determined by load-displacement plots. The critical value of Gaussian curvature at the centre of the plate is determined by the Southwell plot method. The critical value of Gaussian curvature is found to occur before the bifurcation point. Gaussian curvature is found to vary by an order of magnitude over the plate at bifurcation.

Table of Contents

Abstract	ii
Table of Contents	iii
List of Tables	v
List of Figures	vi
List of Symbols	viii
Acknowledgement	x
1 Introduction	1
1.1 Purpose	1
1.2 Literature Review	2
2 Theory	3
2.1 Physics of the Problem	3
2.2 Finite Element Theory	6
2.3 Plate Theory	8
2.4 Southwell Plot	9
3 Analysis	10
3.1 Preprocessing	10
3.2 Solution	11

3.3	Postprocessing	12
4	Results	13
4.1	Deflection	13
4.2	Southwell Plot	19
4.3	Gaussian Curvature and Mean Curvature	20
4.4	Curvature	24
4.5	Midsurface Strain	27
4.6	Fixed Plate Centre	30
4.7	Alternate Finite Element	34
4.8	Non-convergence	35
5	Discussions	37
5.1	FEA Comparison of P_{cr} and P_{Kcr}	37
5.2	Comparisons with Bifurcation Points in Literature	39
5.2.1	Howell	39
5.2.2	Ramsey	40
5.2.3	Miyagawa, Hirata, and Shibuya	41
5.2.4	Lee and Hsu	42
6	Conclusions	44
	Bibliography	45

List of Tables

3.1	Material Constants	10
3.2	Plate Geometry	11
4.1	Critical Values from load-deflection plot	16
4.2	Critical Values from load-deflection plot	17
4.3	Critical Values from Southwell plot	20
4.4	Critical Values from Gaussian-mean curvature plot	23
4.5	Critical Values from Gaussian-mean curvature plot	24
4.6	SHELL43 Element Critical Values from Southwell plot	35
4.7	SHELL43 Element Critical Values from Southwell plot	35
5.1	Comparison of $P_{K_{cr}}$ and P_{cr}	37
5.2	Comparison of Coefficient with Howell	40
5.3	Modified Coefficient	40

List of Figures

2.1 Square Plate Twisted by Corner Forces	3
2.2 Saddle Surface	4
2.3 Cylindrical Surface	4
2.4 Mohr's Circle for Curvature	5
3.1 Constraints	11
4.1 Deflection Contour Plot for 3 pinned corners at P_{cr}	14
4.2 Load-Deflection Plot for 3 pinned corners	14
4.3 Deflection Contour Plot for 3 pinned corners (rotated) at P_{cr}	15
4.4 Load-Deflection Plot for 3 pinned corners (rotated) with varying a/h ratios	16
4.5 Load-Deflection Plot for 3 pinned corners (rotated) with varying mesh density	17
4.6 Deflection Contour Plot for 3 pinned corners (rotated) at $P_{cr}/2$	18
4.7 Deflection Contour Plot for 3 pinned corners (rotated) at $2P_{cr}$	18
4.8 Southwell Plot	19
4.9 Critical Value of Gaussian Curvature from Southwell plot	21
4.10 Coefficient from Southwell plot	21
4.11 Gaussian-Mean Curvature Plot	22
4.12 Load-Gaussian Curvature Plot	22
4.13 Load-Mean Curvature Plot	23
4.14 Gaussian Curvature Contour Plot at P_{Kcr}	25
4.15 Gaussian Curvature Contour Plot at P_{cr}	25

4.16	Mean Curvature Contour Plot at $P_{K_{cr}}$	26
4.17	Mean Curvature Contour Plot at P_{cr}	26
4.18	Load-Curvature Plot	27
4.19	Curvature κ_x Contour Plot at $P_{K_{cr}}$	28
4.20	Curvature κ_x Contour Plot at P_{cr}	28
4.21	Twist κ_{xy} Contour Plot at $P_{K_{cr}}$	29
4.22	Twist κ_{xy} Contour Plot at P_{cr}	29
4.23	Midsurface Strain Plot	30
4.24	Midsurface Strain ϵ_x Contour Plot at $P_{K_{cr}}$	31
4.25	Midsurface Strain ϵ_x Contour Plot at P_{cr}	31
4.26	Midsurface Strain γ_{xy} Contour Plot at $P_{K_{cr}}$	32
4.27	Midsurface Strain γ_{xy} Contour Plot at P_{cr}	32
4.28	Load-Deflection Plot for fixed plate centre	33
4.29	Load-Gaussian Curvature Plot for fixed plate centre	34
5.1	Load-Gaussian Curvature Plot	38
5.2	Load-Deflection Plot	38
5.3	Load-Deflection Plot	41

List of Symbols

a	plate length
C	coefficient for the critical value of twist
C_a, C_b, C_c, C_d	plate corners
D	plate flexural rigidity
E	Young's modulus of elasticity
h	plate thickness
P	corner force
\bar{P}	nondimensionalised corner force
P_{cr}	corner force at bifurcation
P_{Kcr}	corner force at critical value of Gaussian curvature (from Gaussian-mean curvature plot)
P_{Scr}	corner force at critical value of Gaussian curvature (from Southwell plot)
u, v, w	displacement
δ_c	deflection at corner C_c of plate
δ_o	deflection at centre of plate

$\bar{\delta}$	nondimensionalised deflection
$\epsilon_x, \epsilon_y, \gamma_{xy}$	strain
κ_x, κ_y	curvature of the surface
κ, κ_{xy}	twist of the surface
K	Gaussian curvature
K_{cr}	critical value of Gaussian curvature
μ	mean curvature
ν	Poisson's ratio

Acknowledgement

The author would like to thank Professor Hilton Ramsey for his guidance during the researching and writing of this thesis.

The author would also like to thank the Natural Sciences and Engineering Research Council of Canada for their financial support.

Chapter 1

Introduction

1.1 Purpose

The purpose of this work is to investigate the buckling of a linear elastic, isotropic square plate twisted by corner forces, by determining the bifurcation point. The problem is examined by a nonlinear finite element buckling analysis using the commercially available software package ANSYS Revision 5.0. A square plate twisted by corner forces is described by classical linear theory as a saddle surface. In an experiment, as the plate deforms to any noticeable deflection, it appears not as a saddle surface, but as a cylindrical surface. The transformation in mode shapes presents problems in determining material behaviour in shear by experiment. The findings of the present FEA work can be used in future study to develop a nonlinear relationship to account for this transformation and/or an upper bound to the application of a plate twist experiment. The two mode shapes can be described by either displacement or curvature of the surface. The critical value of corner force at bifurcation is determined from load-displacement plots. The critical value of Gaussian curvature at the centre of the plate is determined from the Southwell plot method. There is a discrepancy in the results found in literature using different methods of analysis and assumptions. The present FEA work is compared to the experimental results of Howell and other results in literature.

1.2 Literature Review

In 1890, Kelvin and Tait noted a transition in deformation surfaces of a square plate twisted by corner forces but did not attempt to find the point of instability.

In 1971, Lee and Hsu[2] investigated the buckling problem numerically, using finite difference methods and the nonlinear von Kármán equations for plates. The critical value of corner force at bifurcation was determined by displacement-load plots.

In 1975, Miyagawa, Hirata, and Shibuya[3] investigated the buckling problem experimentally and numerically, using deflection measurements in the experimental approach, and using a polynomial deformed configuration, von Kármán theory, and stress functions in the numerical approach. The critical value of corner force at bifurcation was determined by load-deflection plots.

In 1985, Ramsey[5] investigated the buckling problem analytically, using the kinematic results of Green and Naghdi for small deformations superposed on a large deformation of an elastic Cosserat surface, and the restricted form of the general nonlinear theory of shells and plates of Naghdi. The critical value of twist at bifurcation was determined from a Rayleigh quotient.

In 1991, Howell[1] investigated the buckling problem experimentally, using strain measurements and Kirchhoff theory to determine curvatures. The critical value of Gaussian curvature at bifurcation was determined by the Southwell plot.

Chapter 2

Theory

2.1 Physics of the Problem

Classical linear theory of flat plates describes deflection w of a square plate twisted by corner forces P (figure 2.1):

$$w = \frac{P}{2(1-\nu)D}xy \quad (2.1)$$

in terms of the surface coordinates of the plate x, y . Flexural rigidity of the plate D :

$$D = \frac{Eh^3}{12(1-\nu^2)} \quad (2.2)$$

is a function of Young's modulus of elasticity E , Poisson's ratio ν , and plate thickness h .

Deflection can also be expressed in terms of twist κ of the surface:

$$w = \kappa xy \quad (2.3)$$

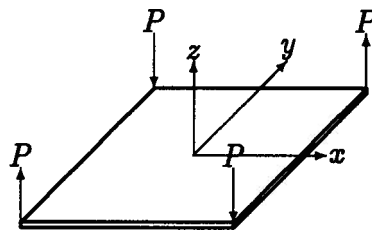


Figure 2.1: Square Plate Twisted by Corner Forces

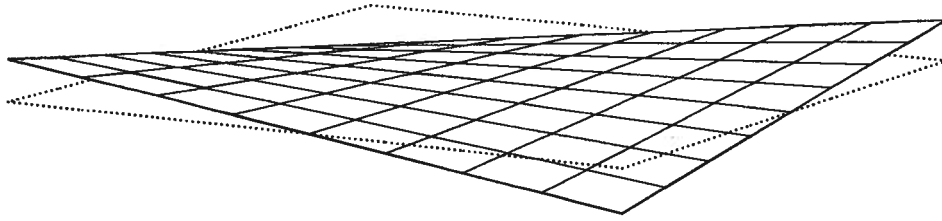


Figure 2.2: Saddle Surface

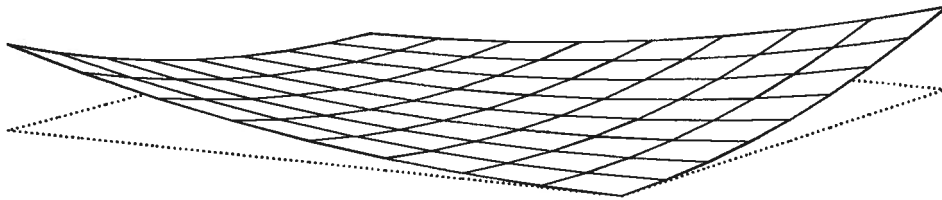


Figure 2.3: Cylindrical Surface

These results (equations 2.1, 2.3) are well known in fundamental classical linear plate theory. The plate appears as a saddle surface (figure 2.2).

However, in an experiment, as the plate deforms to any noticeable deflection, it appears not as a saddle surface, but as a cylindrical surface with generators parallel to a plate diagonal (figure 2.3).

The mode of the plate can be determined by the surface characteristics with either displacement or curvature attributes. The saddle surface has equal magnitude deflections in the four corners relative to a fixed centre. The cylindrical surface has equal magnitude deflections in two opposite corners and zero deflection in the other two corners relative to a fixed centre.

Curvature can be viewed on a Mohr's circle for curvature (figure 2.4). The abscissa



Figure 2.4: Mohr's Circle for Curvature

represents curvature κ_n and the ordinate represents twist κ_{nt} of the surface. Principal curvatures are κ_1, κ_2 . The saddle surface is anticlastic—the two principal curvatures have opposite signs (figure 2.4a). Principal directions are parallel to the plate diagonals. Principal curvatures are equal and opposite, resulting in zero mean curvature and negative Gaussian curvature. The cylindrical surface is synclastic—curvatures in all orientations have like signs (figure 2.4b). Principal directions are parallel to the plate diagonals. One principal curvature is zero and the other non-zero, resulting in a non-zero mean curvature and a zero Gaussian curvature.

Classical linear theory of flat plates neglects all quadratic terms in the Green-Lagrange strain:

$$\epsilon_x = u_x + \frac{1}{2}(u_x^2 + v_x^2 + w_x^2) \quad (2.4)$$

$$\epsilon_y = v_y + \frac{1}{2}(u_y^2 + v_y^2 + w_y^2) \quad (2.5)$$

$$\epsilon_z = w_z + \frac{1}{2}(u_z^2 + v_z^2 + w_z^2) \quad (2.6)$$

$$\gamma_{xy} = v_x + u_y + (u_x u_y + v_x v_y + w_x w_y) \quad (2.7)$$

$$\gamma_{yz} = w_y + v_z + (u_y u_z + v_y v_z + w_y w_z) \quad (2.8)$$

$$\gamma_{zx} = u_z + w_x + (u_x u_z + v_x v_z + w_x w_z) \quad (2.9)$$

The approximation of neglecting the nonlinear terms fails to account for the deformation in the middle plane of the plate due to bending. Midsurface strains can only

be neglected if the deflections of the plate are small in comparison with its thickness in non-developable surfaces (non-zero Gaussian curvature, such as saddle shapes, spheres) or the deflections are of the order of its thickness in developable surfaces (zero Gaussian curvature, such as cylinders, cones)[9]. Because of this approximation, classical linear plate theory cannot predict buckling.

2.2 Finite Element Theory

The finite element used in the analysis is an 8 node isoparametric quadrilateral shell element. It is labeled SHELL93 in the ANSYS Revision 5.0 element library. There are 5 degrees of freedom per node: 3 translations and 2 rotations. This element includes features of Green-Lagrange strains and Mindlin plate theory. Green-Lagrange strains (equations 2.4–2.9) take into account midsurface strains of the plate. Mindlin plate theory allows for transverse shear deformation. This means that a line that is straight and normal to the midsurface before loading, is assumed to remain straight but not necessarily normal to the midsurface after loading. Displacements u , v of a point in the plate a distance z from the midsurface are:

$$u = \bar{u} - z\alpha \quad (2.10)$$

$$v = \bar{v} - z\beta \quad (2.11)$$

where α , β are small angles of rotation of a line that was normal to the midsurface before loading and \bar{u} , \bar{v} are the displacements at the plate midsurface. Strains ϵ_x , ϵ_y and shear strains γ_{xy} , γ_{yz} , γ_{zx} are:

$$\epsilon_x = \bar{u}_x + \frac{1}{2}(\bar{u}_x^2 + \bar{v}_x^2 + w_x^2) - z\alpha_x \quad (2.12)$$

$$\epsilon_y = \bar{v}_y + \frac{1}{2}(\bar{u}_y^2 + \bar{v}_y^2 + w_y^2) - z\beta_y \quad (2.13)$$

$$\gamma_{xy} = \bar{v}_x + \bar{u}_y + (\bar{u}_x\bar{u}_y + \bar{v}_x\bar{v}_y + w_x w_y) - z(\beta_x + \alpha_y) \quad (2.14)$$

$$\gamma_{yz} = w_y + \bar{v}_z + (\bar{u}_y \bar{u}_z + \bar{v}_y \bar{v}_z + w_y w_z) - \beta \quad (2.15)$$

$$\gamma_{zx} = \bar{u}_z + w_x + (\bar{u}_z \bar{u}_x + \bar{v}_z \bar{v}_x + w_z w_x) - \alpha \quad (2.16)$$

Strains ϵ_x , ϵ_y and shear strain γ_{xy} are assumed to vary linearly through the plate thickness. Transverse shear strains γ_{yz} , γ_{zx} are assumed to be constant through the plate thickness.

In the stress-strain relationship:

$$\{\sigma\} = [D] \{\epsilon\} \quad (2.17)$$

the stress vector $\{\sigma\}$, the strain vector $\{\epsilon\}$, and the material property matrix for the element $[D]$ are defined as:

$$\{\sigma\} = \begin{bmatrix} \sigma_x & \sigma_y & \tau_{xy} & \tau_{yz} & \tau_{zx} \end{bmatrix}^T \quad (2.18)$$

$$\{\epsilon\} = \begin{bmatrix} \epsilon_x & \epsilon_y & \gamma_{xy} & \gamma_{yz} & \gamma_{zx} \end{bmatrix}^T \quad (2.19)$$

$$[D] = \frac{E}{1-\nu^2} \begin{bmatrix} 1 & \nu & 0 & 0 & 0 \\ \nu & 1 & 0 & 0 & 0 \\ 0 & 0 & \frac{1-\nu}{2} & 0 & 0 \\ 0 & 0 & 0 & \frac{1-\nu}{2f} & 0 \\ 0 & 0 & 0 & 0 & \frac{1-\nu}{2f} \end{bmatrix} \quad (2.20)$$

where f is the shear factor:

$$f = \begin{cases} 1.2, & A/h^2 \leq 25 \\ 1.0 + 0.2 \frac{A}{25h^2}, & A/h^2 > 25 \end{cases} \quad (2.21)$$

where A is the area of the element and h is the plate thickness. The shear factor is designed to avoid shear locking. As the element becomes thin, the A/h^2 ratio becomes large. The shear factor f is thus increased and the stiffness associated with the transverse shears is reduced. The correct method to avoid shear locking is through selective integration, but ANSYS does not accommodate this. The SHELL93 element uses a 2×2 reduced quadrature rule.

2.3 Plate Theory

Kirchhoff theory is used to calculate curvatures from strain output of the finite element software. This is to be consistent with Howell's experimental analysis so results can be compared. Kirchhoff theory neglects transverse shear deformations. This means that a line that is straight and normal to the midsurface before loading, is assumed to remain straight and normal to the midsurface after loading.

Extensional strain ϵ_s at an arbitrary point a distance z from the plate midsurface is:

$$\epsilon_s = \epsilon_m + z\kappa \quad (2.22)$$

where the membrane strain ϵ_m appears along the plate midsurface, and the curvature κ is associated with bending strain.

Solving the above equation for the top and bottom of the plate and equating midsurface strains gives the curvatures κ_x , κ_y and the twist κ_{xy} of the midsurface:

$$\kappa_x = \frac{\epsilon_x^t - \epsilon_x^b}{h} \quad (2.23)$$

$$\kappa_y = \frac{\epsilon_y^t - \epsilon_y^b}{h} \quad (2.24)$$

$$\kappa_{xy} = \frac{\gamma_{xy}^t - \gamma_{xy}^b}{2h} \quad (2.25)$$

where ϵ^t , ϵ^b are the top and bottom surface strains of the plate respectively, and h is the plate thickness.

Principal curvatures κ_1 , κ_2 from Mohr's circle of curvatures are:

$$\kappa_1, \kappa_2 = \frac{\kappa_x + \kappa_y}{2} \pm \sqrt{\left(\frac{\kappa_x - \kappa_y}{2}\right)^2 + \kappa_{xy}^2} \quad (2.26)$$

Mean curvature μ is the average of the two principal curvatures:

$$\mu = \frac{1}{2}(\kappa_x + \kappa_y) = \frac{1}{2}(\kappa_1 + \kappa_2) \quad (2.27)$$

Gaussian curvature K is product of the two principal curvatures:

$$K = \kappa_x \kappa_y - \kappa_{xy}^2 = \kappa_1 \kappa_2 \quad (2.28)$$

2.4 Southwell Plot

The Southwell plot is a common method to determine the elastic buckling load of a structural system. In experiments, there exists some imperfection in the undeformed shape and/or applied loading. As the compressive load increases, the lowest critical load buckling mode dominates. A linear function can be expressed in terms of applied load and deflection by neglecting contributions from higher modes.

In 1932, Southwell considered a simply supported column with an initial imperfection subjected to a compressive load P [6]. He expressed a linear relationship:

$$\frac{\delta}{P} = \frac{1}{P_{cr}} \delta + \frac{1}{P_{cr}} a \quad (2.29)$$

in terms of the incremental deflection δ , the Euler load P_{cr} , and coefficient a . The Southwell plot of δ/P versus δ gives a straight line whose slope is equal to the inverse of the buckling load.

The Southwell plot method claims accuracy only as $P \rightarrow P_{cr}$. Spencer[7] states that constructing Southwell plots using Kármán's strut data with loads up to $0.91P_{cr}$, to $0.88P_{cr}$, and to $0.82P_{cr}$ (P_{cr} being defined as the critical load which Southwell obtained by plotting Kármán's data to $0.98P_{cr}$) gives errors of 3, 5, and 25 percent respectively.

The critical load P_{cr} is a theoretical concept and should be independent of initial deflection. Spencer[7] showed that in buckling of a uniaxially compressed simply supported plate, the Southwell plot begins to underestimate the critical load when:

$$w_o/h > 0.5 \quad (2.30)$$

where w_o is the initial deflection at the plate centre and h is the plate thickness.

Chapter 3

Analysis

The analysis was performed on a SUN SPARC workstation. The preprocessing and the solution utilized ANSYS Revision 5.0, and the postprocessing utilized FORTRAN77 and TECPLOT Revision 5.0.

3.1 Preprocessing

The plate is modelled with the SHELL93 8 node isoparametric shell element.

The plate material is modelled as T6061-T6 Aluminium (table 3.1) for comparison with the experimental results of Howell[1]. Material nonlinearity, such as plasticity, is not considered in the analysis.

The plate geometry is square with plate length to thickness ratios a/h (table 3.2) for comparison with the experimental results of Howell[1].

The plate is meshed with square elements N per side, where N is even to provide a node at the centre of the plate to take displacement and strain measurements—the same location as Howell's strain gauges[1]. There are a total of N^2 elements and $(3N^2 + 4N + 1)$ nodes for the model.

Table 3.1: Material Constants

E	69×10^9	Pa
ν	0.33	

Table 3.2: Plate Geometry

a/h ratio	a (m)	h (m)
49.2	0.1524	0.003099
63.2	0.2032	0.003216
80.3	0.2540	0.003162
96.0	0.3048	0.003175
196.7	0.6096	0.003099

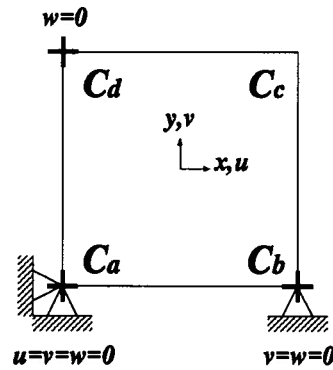


Figure 3.1: Constraints

3.2 Solution

The plate is constrained at corners C_a , C_b , C_d (figure 3.1) to zero displacement in the z direction, to simulate the self equilibrating corner forces associated with the applied force at corner C_c . These are the same constraints in the experiment by Howell[1]. To prevent rigid body motion, additional DOF constraints are specified. The plate is constrained at corner C_a to zero displacement in the x and y directions to prevent translation, and constrained at corner C_b to zero displacement in the y direction to prevent rotation. These constraints satisfy the kinematic, but not the static boundary conditions of a plate with free edges.

When applying the Southwell plot method to find critical values, an initial hydrostatic

pressure is applied in the positive z direction. A nominal value of hydrostatic loading is used which produces deflections small compared to the plate thickness.

The applied force P at corner C_c is in the positive z direction.

These boundary conditions provide a stable post buckling response. The applied corner force P can exceed the value at the bifurcation point P_{cr} without the instability of ill conditioned matrices, such as a negative main diagonal in the stiffness matrix.

Body forces, such as gravity loads, are not included in the analysis.

3.3 Postprocessing

Displacements δ_o , δ_c are calculated at the centre of the plate and at corner C_c . The critical value of corner force at bifurcation is determined from load-deflection plot.

Strains ϵ_x , ϵ_y , γ_{xy} are calculated at the top and bottom surfaces at the node at the centre of the plate using nodal point averaging in ANSYS. These values are exported to a FORTRAN code which calculates curvatures using Kirchhoff plate theory. The critical value of Gaussian curvature K_{cr} is determined from the Southwell plot. The Southwell plot uses μ as the abscissa and μ/K as the ordinate. The asymptotic behaviour of the curve determines K_{cr} as $K/K_{cr} \rightarrow 1$.

Chapter 4

Results

4.1 Deflection

The deflection for the plate with 3 pinned corners is zero at the pinned corners C_a , C_b , C_d and a maximum at the corner with the applied force C_c (figure 4.1).

The load-deflection curve of corner with the applied force C_c is smooth and shows no indication of buckling (figure 4.2). The load-deflection curve of the centre of the plate has an abrupt change in the slope at the bifurcation point P_{cr} .

The finite element analysis deflection of the plate centre agrees well with linear theory (equation 2.1) for deflections less than a plate thickness (figure 4.2). The FEA deflection of the plate corner C_c agrees well with linear theory for deflections less than 4 plate thicknesses.

The finite element results of the plate with 3 pinned corners can be rotated to show the characteristic surface. The plate can be rotated so the deflections of corners C_a and C_c are equal, and translated so the deflection of the centre of the plate is zero. The deflections become $\delta_c/2 - \delta_o$ at C_a and C_c , and $-\delta_o$ at C_b and C_d (figure 4.3), where δ_o and δ_c are the deflections of the unrotated results for the centre of the plate and corner C_c respectively.

The bifurcation point is where the magnitude of rotated corners C_a , C_c and rotated corners C_b , C_d significantly diverge. The critical value of corner load varies slightly with Howell's[1] a/h ratios (figure 4.4 and table 4.1). The mesh density of 144 elements is

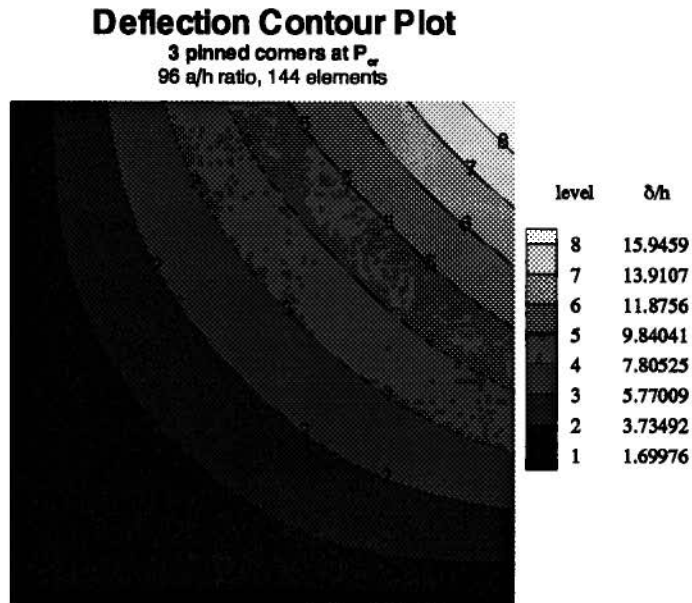


Figure 4.1: Deflection Contour Plot for 3 pinned corners at P_{cr}

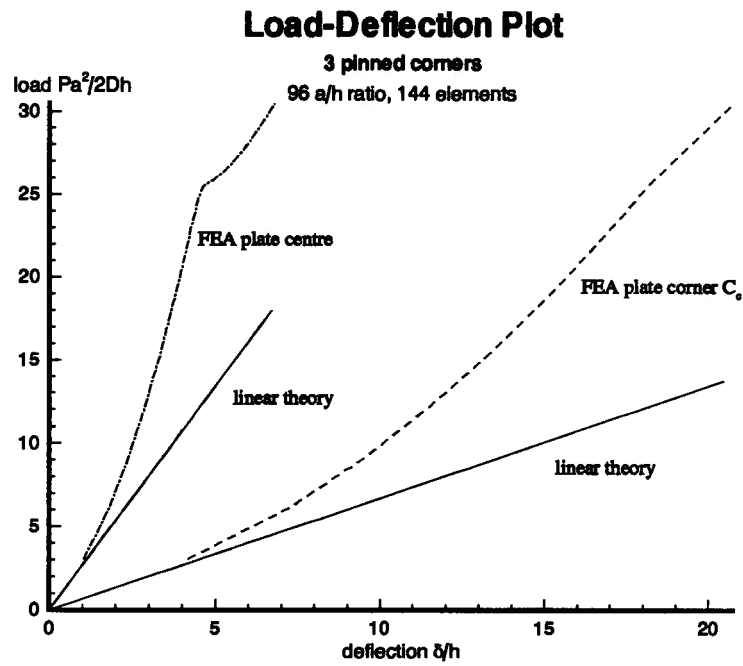


Figure 4.2: Load-Deflection Plot for 3 pinned corners

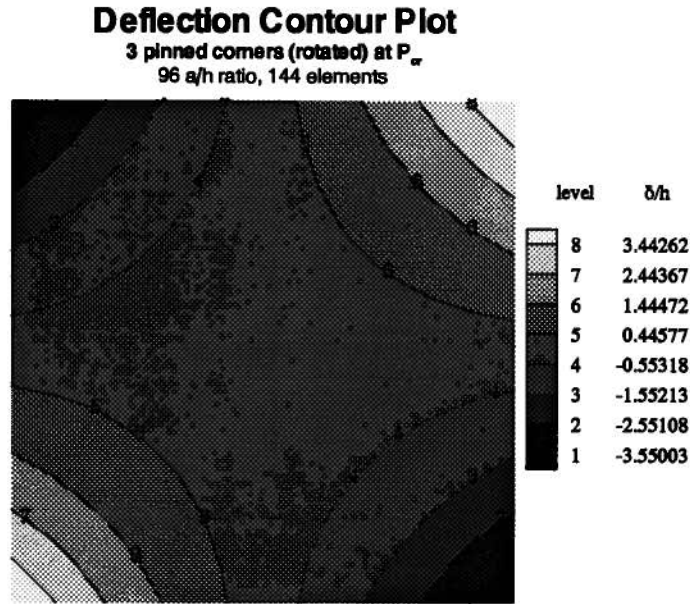


Figure 4.3: Deflection Contour Plot for 3 pinned corners (rotated) at P_{cr}

sufficient to provide displacement convergence (figure 4.5 and table 4.2).

Below the bifurcation point, the magnitudes of deflection for rotated corners C_a , C_c and rotated corners C_b , C_d are almost equal (figure 4.4). The plate is bending to a saddle surface (figure 4.6).

Above the bifurcation point, the magnitude of deflection for rotated corners C_a , C_c is decreasing, and the magnitude of deflection for rotated corners C_b , C_d is increasing. (figure 4.4). The plate is bending to a cylindrical surface (figure 4.7).

Nondimensionalized corner force \bar{P} is defined as[3]:

$$\bar{P} = \frac{Pa^2}{2Dh} \quad (4.1)$$

Nondimensionalized deflection $\bar{\delta}$ is defined as[3]:

$$\bar{\delta} = \frac{\delta}{h} \quad (4.2)$$

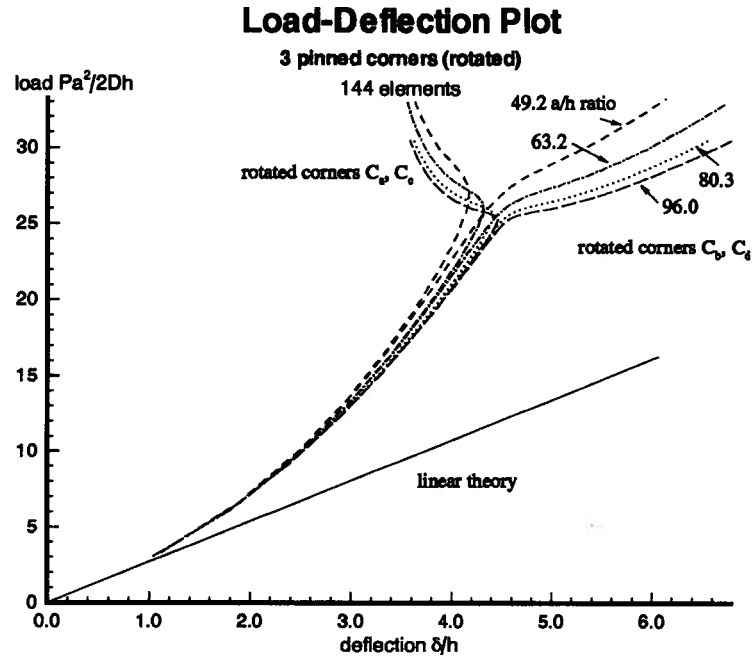
Figure 4.4: Load-Deflection Plot for 3 pinned corners (rotated) with varying a/h ratios

Table 4.1: Critical Values from load-deflection plot

144 elements				
a/h ratio	P_{cr} (N)	\bar{P}_{cr}	δ_a, δ_c	δ_b, δ_d
49.2	1380	26.9	4.17	4.48
63.2	870	26.0	4.32	4.52
80.3	510	25.5	4.41	4.53
96.0	355	25.1	4.45	4.55
196.7	80	24.9	4.54	4.58

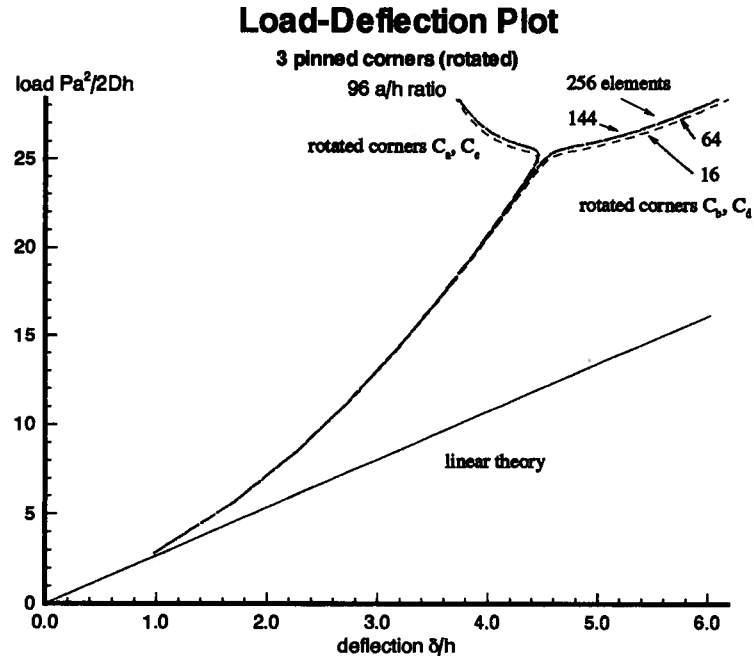
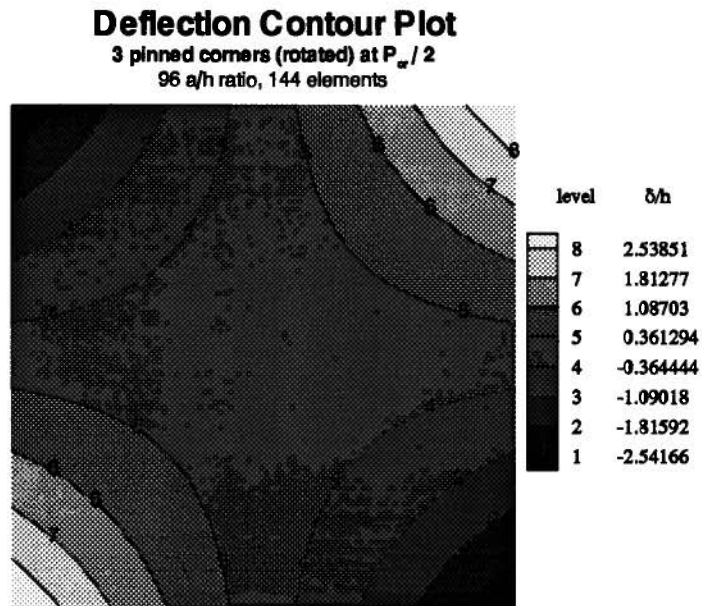
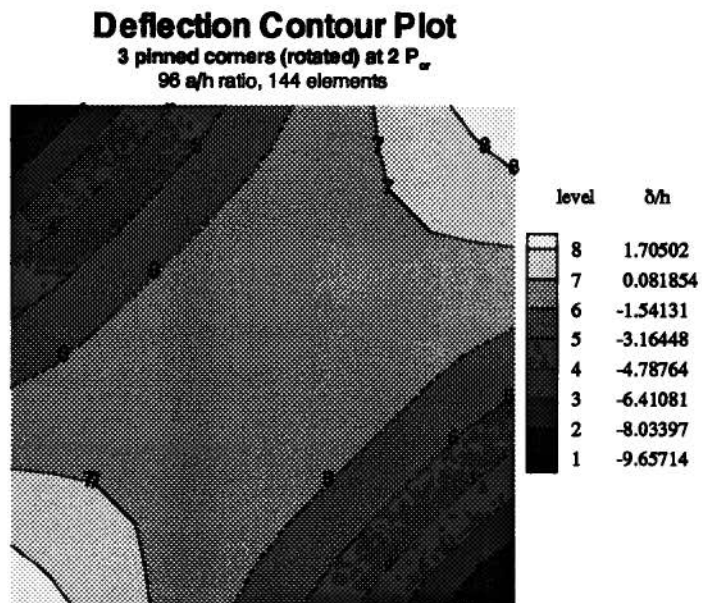


Figure 4.5: Load-Deflection Plot for 3 pinned corners (rotated) with varying mesh density

Table 4.2: Critical Values from load-deflection plot

96 a/h ratio				
elements	P_{cr} (N)	\bar{P}_{cr}	δ_a, δ_c	δ_b, δ_d
16	352	25.0	4.45	4.55
64	355	25.1	4.45	4.55
144	355	25.1	4.45	4.55
256	355	25.1	4.45	4.55

Figure 4.6: Deflection Contour Plot for 3 pinned corners (rotated) at $P_{cr}/2$ Figure 4.7: Deflection Contour Plot for 3 pinned corners (rotated) at $2P_{cr}$

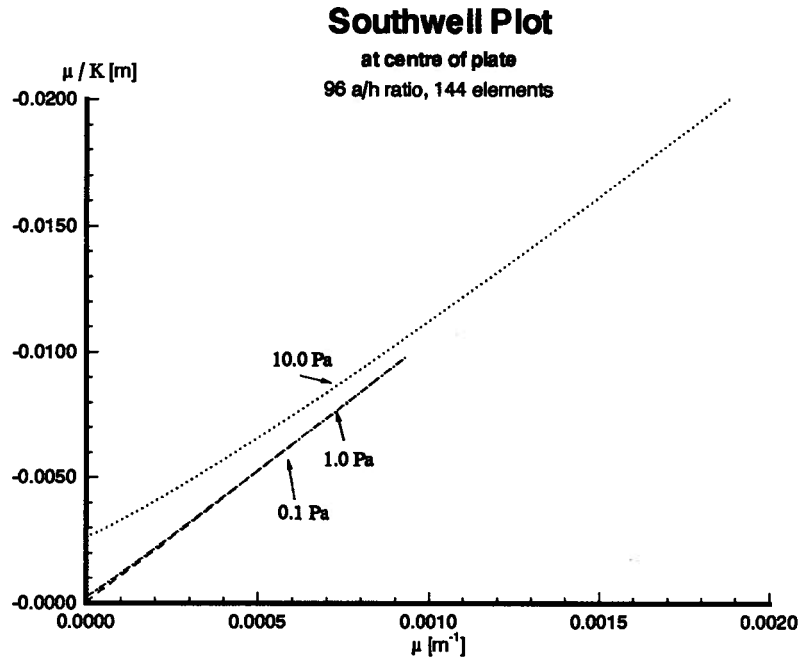


Figure 4.8: Southwell Plot

4.2 Southwell Plot

Howell[1] determined the critical value of Gaussian curvature using the Southwell plot method. The Southwell plot method requires an initial curvature in the structure.

The FEA Southwell plot is constructed from strains at the centre of the plate with 3 pinned corners and initial hydrostatic pressure. The Southwell plot produces parallel lines for varying intensity of initial hydrostatic pressure (figure 4.8).

The initial hydrostatic pressure creates an initial deflection of the centre of the plate δ_o^0 . The critical value of Gaussian curvature K_{Scr} and corner force is P_{Scr} determined by the Southwell plot method are not affected by deflections δ_o^0 less than one tenth of a plate thickness (table 4.3).

The coefficient C is defined as[5]:

$$C = \kappa \frac{a^2}{h} \quad (4.3)$$

Table 4.3: Critical Values from Southwell plot

96 a/h ratio, 144 elements				
pressure (Pa)	$\bar{\delta}_o^0$	P_{Scr} (N)	\bar{P}_{Scr}	C
0.1	0.0000961	284	20.1	9.04
1	0.000961	284	20.1	9.04
10	0.00961	284	20.1	9.03
100	0.0961	274	19.4	9.01
500	0.478	226	16.0	8.65

for the critical value of twist κ at the centre of the plate.

For load levels less than P_{Scr} , the Southwell plot method over or under predicts K_{Scr} (figure 4.9) and C (figure 4.10) depending on the magnitude of the initial deflection.

4.3 Gaussian Curvature and Mean Curvature

The Southwell plot determines the critical value of Gaussian curvature where the slope on the Gaussian-mean curvature plot (figure 4.11) is zero[7]. The Gaussian-mean curvature plot is constructed from strain calculations at the centre of the plate with 3 pinned corners and no initial hydrostatic pressure.

Gaussian curvature is zero for the undeformed plate (no initial curvature), increases in magnitude as the plate deforms to a saddle surface, reaches a maximum value, begins to decrease in magnitude, and after bifurcation decreases in magnitude as the plate deforms to a cylindrical surface (figure 4.12).

Mean curvature is zero for the undeformed plate (no initial curvature) remains zero as the plate deforms to a saddle surface, and after bifurcation increases in magnitude as the plate deforms to a cylindrical surface (figure 4.13).

The corner load at the critical value of Gaussian curvature P_{Kcr} (tables 4.4–4.5) is less than the corner load at bifurcation P_{cr} (figure 4.12).

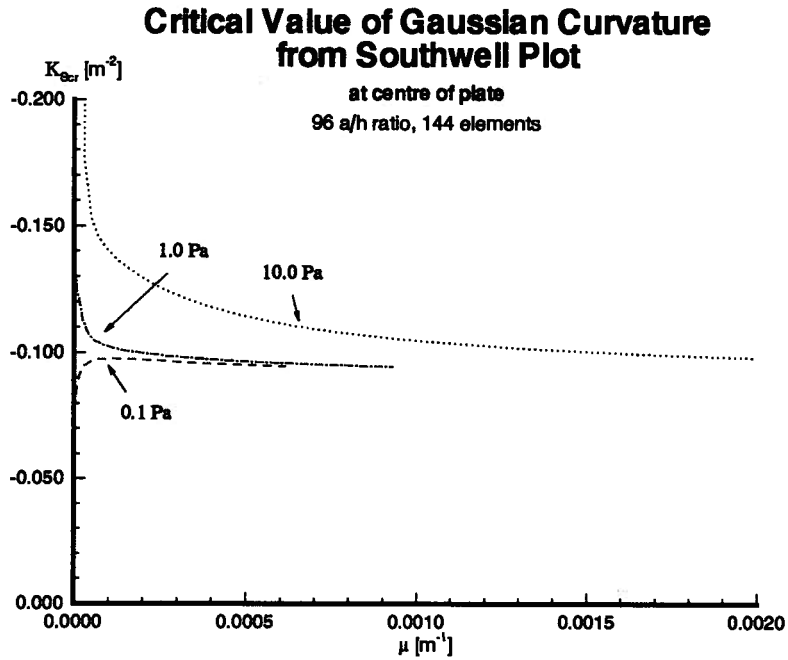


Figure 4.9: Critical Value of Gaussian Curvature from Southwell plot

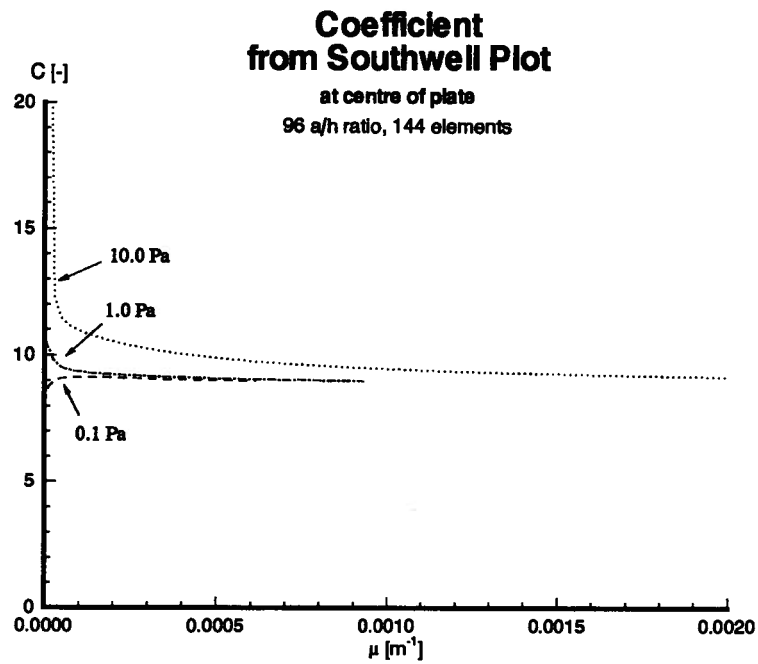


Figure 4.10: Coefficient from Southwell plot

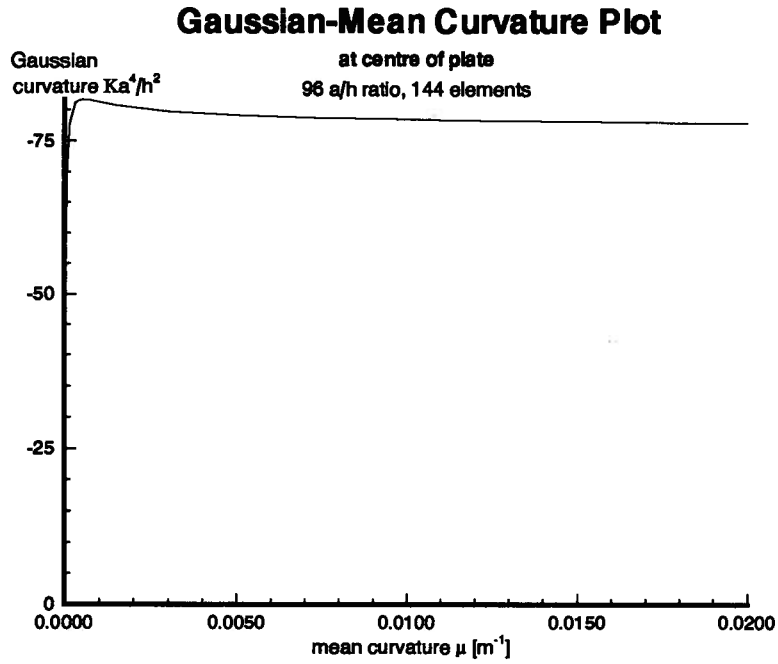


Figure 4.11: Gaussian-Mean Curvature Plot

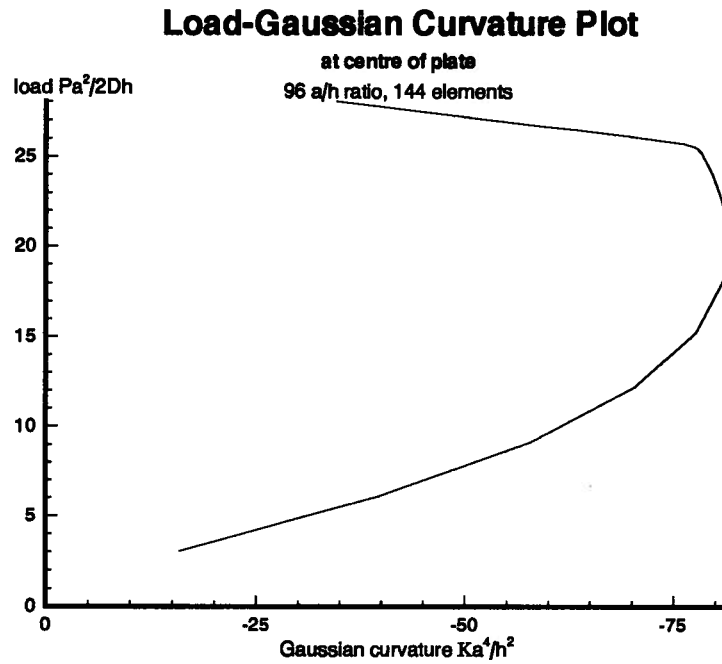


Figure 4.12: Load-Gaussian Curvature Plot

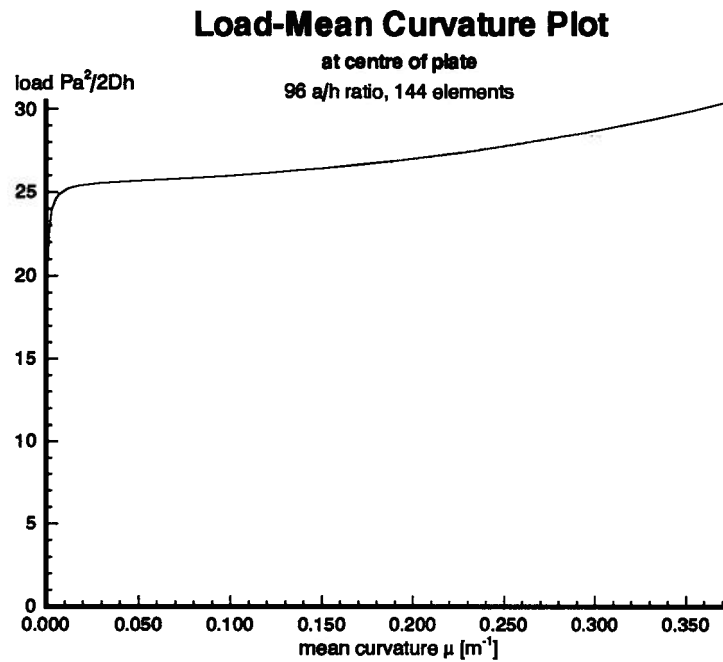


Figure 4.13: Load-Mean Curvature Plot

Table 4.4: Critical Values from Gaussian-mean curvature plot

144 elements			
a/h ratio	P_{Kcr} (N)	\bar{P}_{Kcr}	C
49.2	1112	21.7	9.01
63.2	696	20.8	9.01
80.3	406	20.3	9.02
96.0	284	20.1	9.03
196.7	63	19.7	9.06

Table 4.5: Critical Values from Gaussian-mean curvature plot

96 a/h ratio			
elements	$P_{K_{cr}}$ (N)	$P_{K_{cr}}$	C
16	278	19.7	9.09
64	276	19.6	9.03
144	284	20.1	9.03
256	286	20.3	9.01

Gaussian curvature is a minimum absolute value at the centre of the plate, a maximum absolute value near the corners of the plate, and varies over the plate by an order of magnitude at $P_{K_{cr}}$ (figure 4.14) and P_{cr} (figure 4.15).

Mean curvature is a zero at the centre of the plate and varies positive and negative values over the plate at $P_{K_{cr}}$ (figure 4.16) and P_{cr} (figure 4.17).

4.4 Curvature

The load-curvature plot is constructed from strains at the centre of the plate with 3 pinned corners and no initial hydrostatic pressure. Curvatures κ_x , κ_y are zero for the undeformed plate (no initial curvature), remain zero as the plate deforms to a saddle surface, and after bifurcation increase in magnitude as the plate deforms to a cylindrical surface (figure 4.18).

Twist κ_{xy} is zero for the undeformed plate (no initial curvature), increases in magnitude as the plate deforms to a saddle surface, reaches a maximum value, begins to decrease in magnitude, and after bifurcation continues to increase in magnitude as the plate deforms to a cylindrical surface.

The FEA twist κ_{xy} agrees well with linear theory (equations 2.1–2.3) for deflections less than half the plate thickness, and agrees well with membrane stress theory ([4] and

Gaussian Curvature Contour Plot

at P_{Kcr}
96 a/h ratio, 144 elements

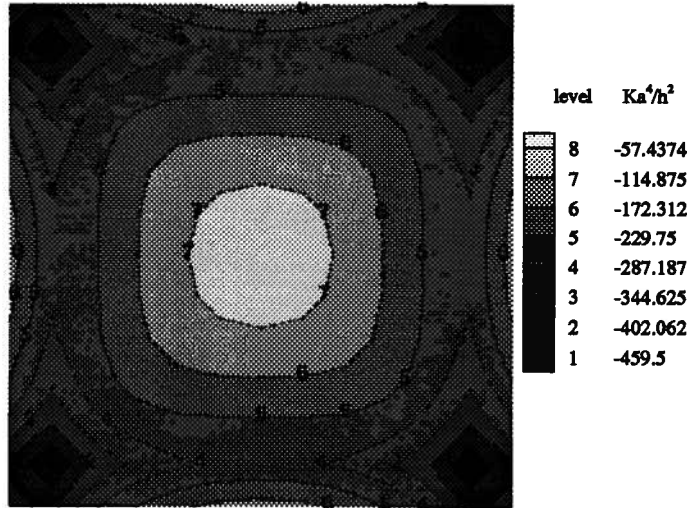


Figure 4.14: Gaussian Curvature Contour Plot at P_{Kcr}

Gaussian Curvature Contour Plot

at P_{cr}
96 a/h ratio, 144 elements

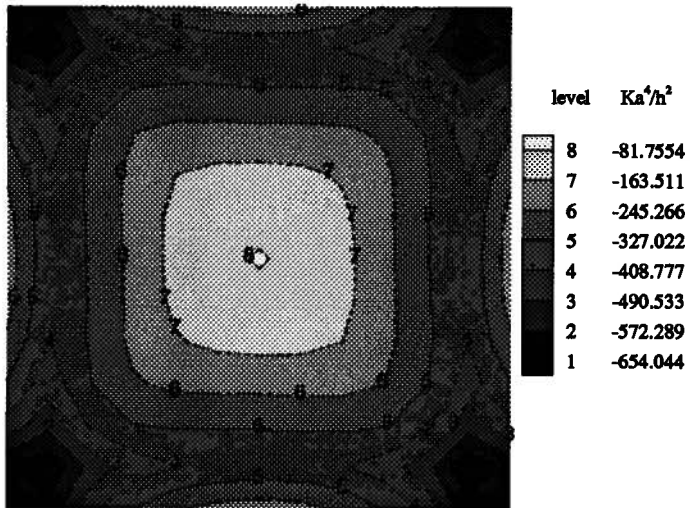


Figure 4.15: Gaussian Curvature Contour Plot at P_{cr}

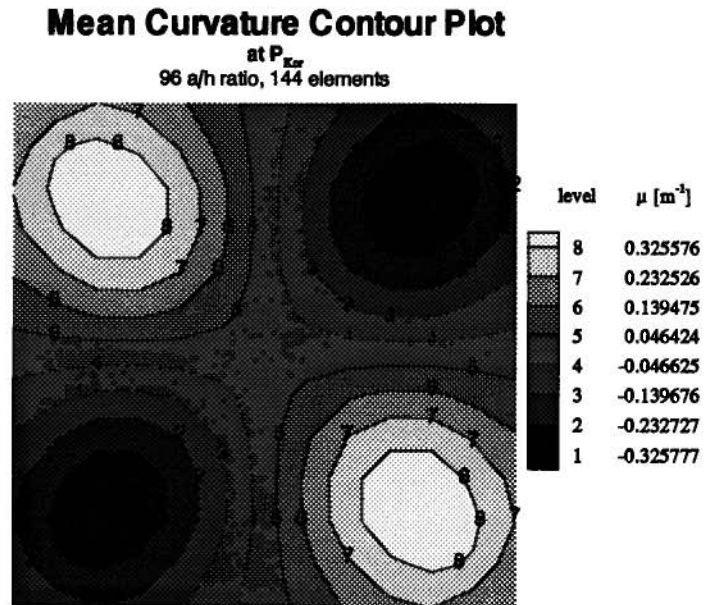


Figure 4.16: Mean Curvature Contour Plot at P_{Kcr}

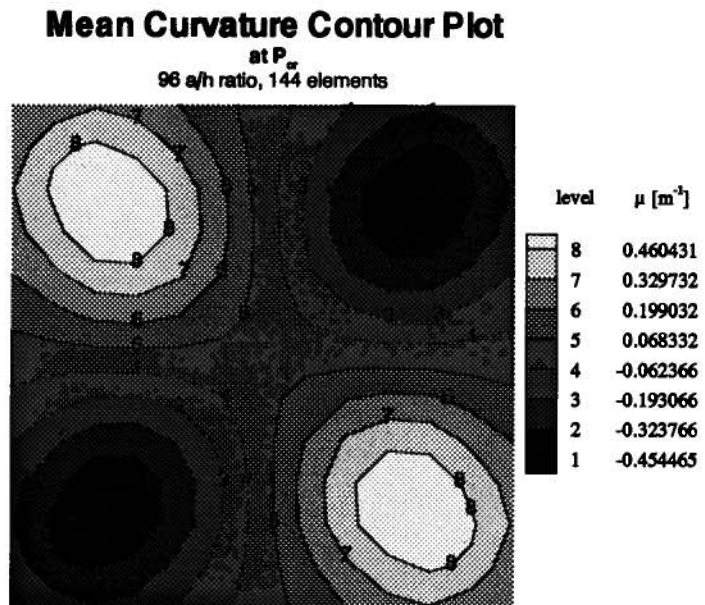


Figure 4.17: Mean Curvature Contour Plot at P_{cr}

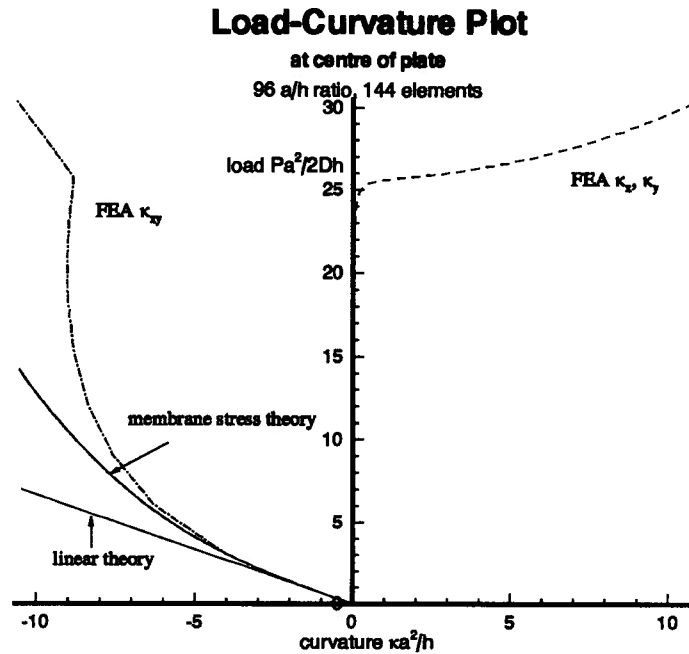


Figure 4.18: Load-Curvature Plot

equation 2.22) for deflections less than a plate thickness (figure 4.18).

Curvature κ_x is a zero at the centre of the plate and varies positive and negative values over the plate at $P_{K_{cr}}$ (figure 4.19) and P_{cr} (figure 4.20).

Twist κ_{xy} is a minimum absolute value at the centre of the plate, a maximum absolute value near the corners of the plate, and varies over the plate by an order of magnitude at $P_{K_{cr}}$ (figure 4.21) and P_{cr} (figure 4.22).

4.5 Midsurface Strain

The load-midsurface strain plot is constructed from strains at the centre of the plate with 3 pinned corners and no initial hydrostatic pressure. Midsurface strains ϵ_x , ϵ_y are zero for the undeformed plate (no initial curvature), are equal and compressive as the plate deforms to a saddle surface, and after bifurcation decrease in magnitude as the plate

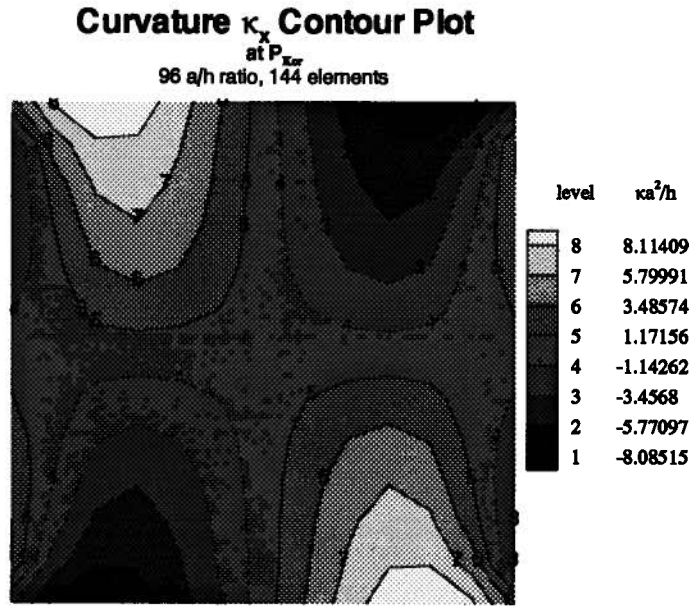


Figure 4.19: Curvature κ_x Contour Plot at P_{Kcr}

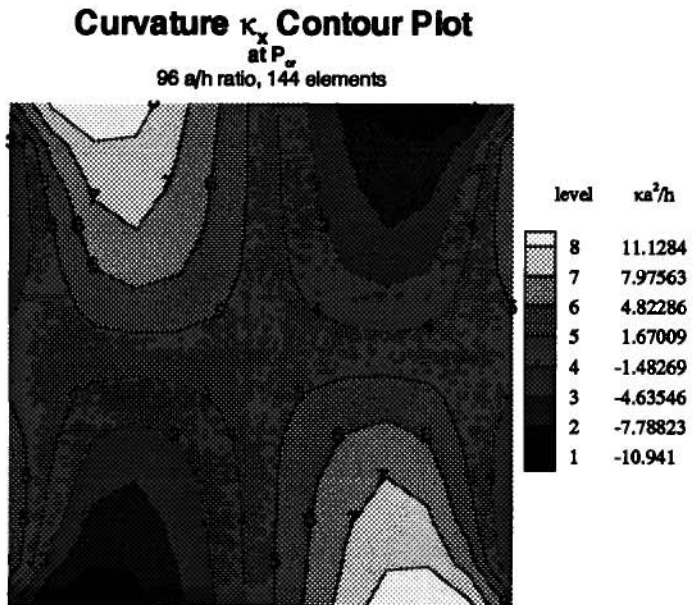


Figure 4.20: Curvature κ_x Contour Plot at P_{cr}

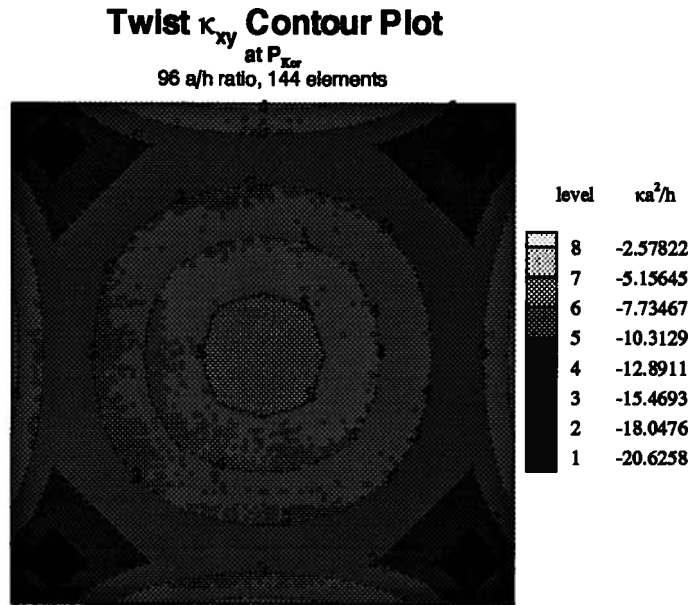


Figure 4.21: Twist κ_{xy} Contour Plot at $P_{K\sigma}$

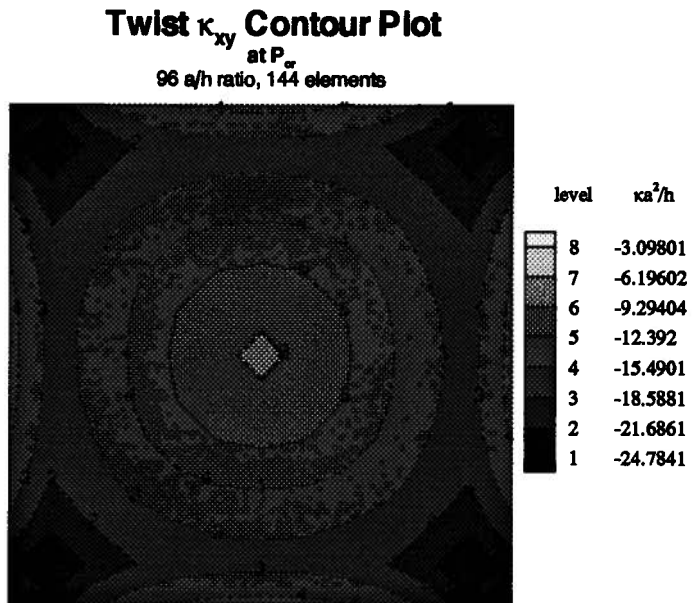


Figure 4.22: Twist κ_{xy} Contour Plot at P_{σ}

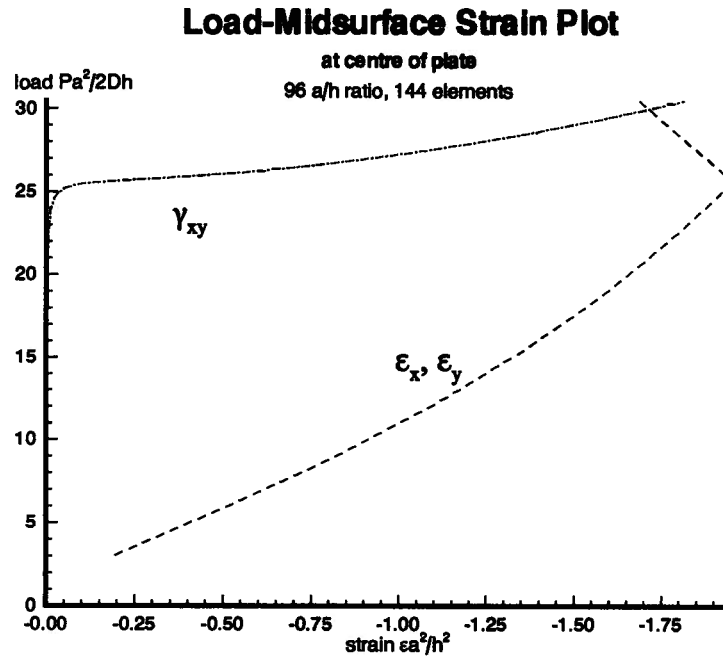


Figure 4.23: Midsurface Strain Plot

deforms to a cylindrical surface (figure 4.23).

Midsurface shear strain γ_{xy} is zero for the undeformed plate (no initial curvature), remains zero as the plate deforms to a saddle surface, and after bifurcation increases in magnitude as the plate deforms to a cylindrical surface.

The midsurface of the plate is in maximum compression at the centre of the plate and maximum tension at the edge of the plate at $P_{K\sigma}$ (figure 4.24) and P_{σ} (figure 4.25).

Midsurface shear strain γ_{xy} is zero at the centre of the plate and varies positive and negative values over the plate at $P_{K\sigma}$ (figure 4.26) and P_{σ} (figure 4.27).

4.6 Fixed Plate Centre

The FEA plate buckles without an initial perturbation because of the 3 pinned corner constraints—the same used by Howell[1]. As the plate deforms only corner C_c is free to

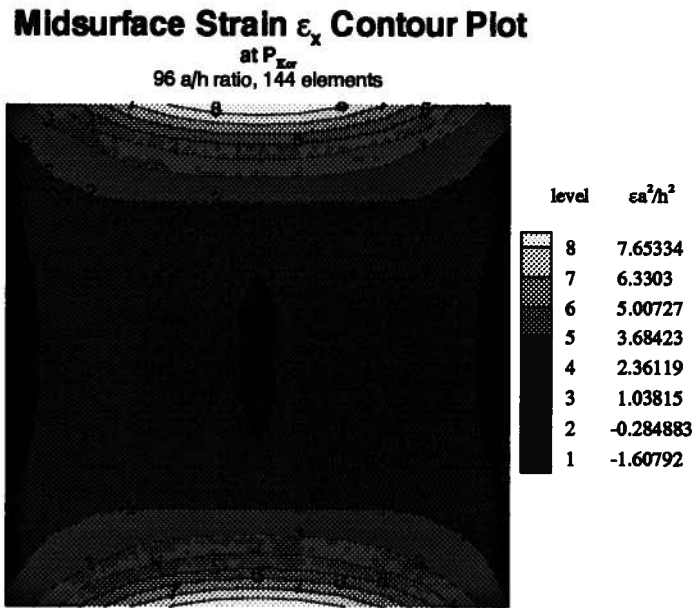


Figure 4.24: Midsurface Strain ϵ_x Contour Plot at P_{Kcr}

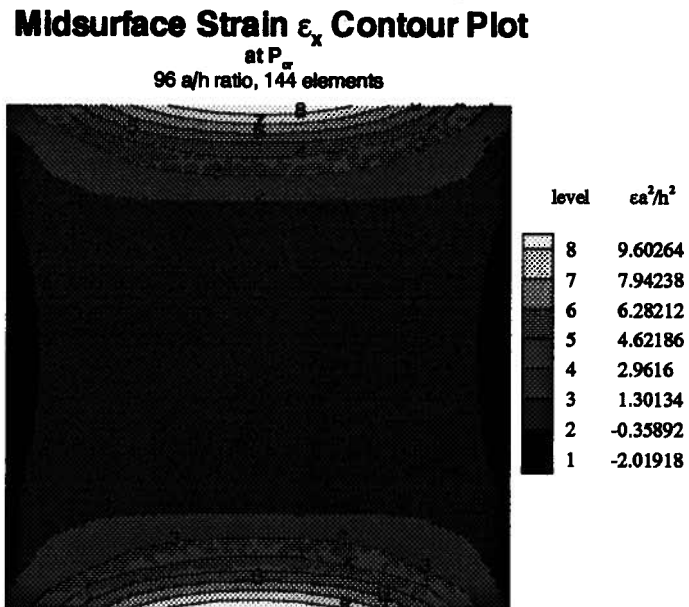


Figure 4.25: Midsurface Strain ϵ_x Contour Plot at P_{cr}

Midsurface Shear Strain γ_{xy} Contour Plot
 at P_{Kcr}
 96 a/h ratio, 144 elements

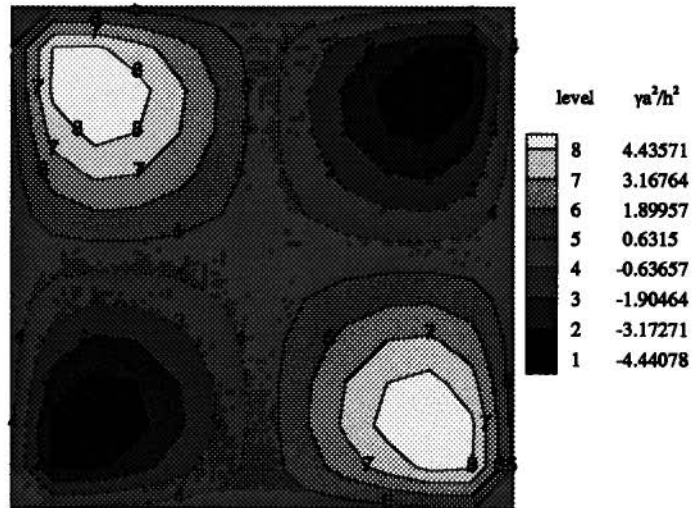


Figure 4.26: Midsurface Strain γ_{xy} Contour Plot at P_{Kcr}

Midsurface Shear Strain γ_{xy} Contour Plot
 at P_{cr}
 96 a/h ratio, 144 elements

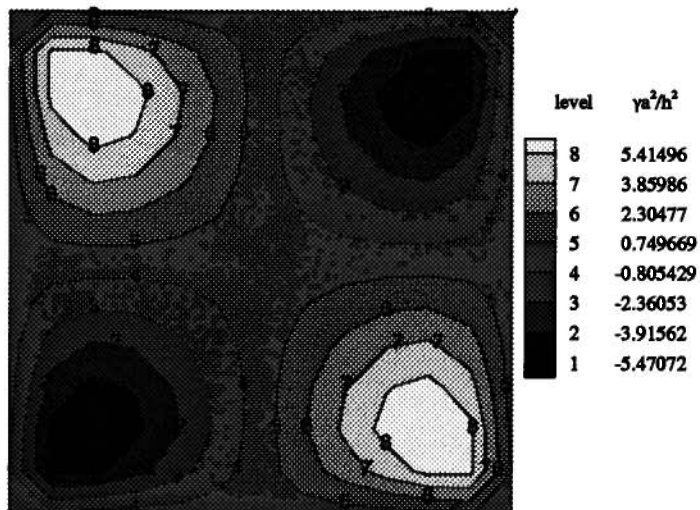


Figure 4.27: Midsurface Strain γ_{xy} Contour Plot at P_{cr}

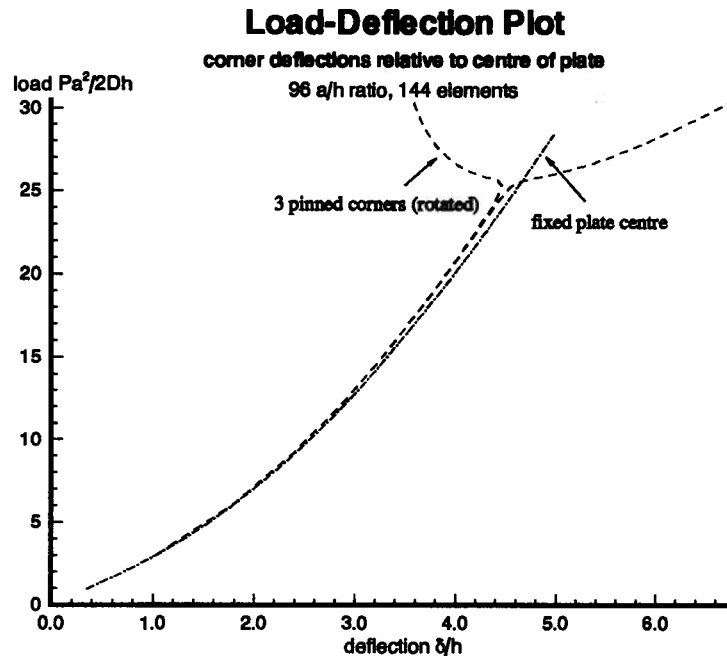


Figure 4.28: Load-Deflection Plot for fixed plate centre

deflect. The corner forces remain parallel to the z axis and are no longer normal to the tangent plane of the centre of the plate.

Constraints which do not initiate buckling are created by fixing the centre of the plate in 5 degrees of freedom: displacements u , v , w and rotations about the x and y axis. The drilling rotation about the z axis is fixed by a constraint on C_a in the direction of the $y = -x$ diagonal. The applied corner loads are P at C_a and C_c and $-P$ at C_b and C_d .

The orientation of the corner forces in the fixed plate centre loading case remain normal to the tangent plane of the centre of the plate. There is no perturbation, and the plate is loaded beyond the bifurcation point without experiencing buckling (figure 4.28).

The critical value of Gaussian curvature remains the same for the 3 pinned corners and the fixed plate centre loading cases (figure 4.29).

The 3 pinned corners and the fixed plate centre loading cases create membrane tension for large deflections due to the corner forces remaining in their original orientation and

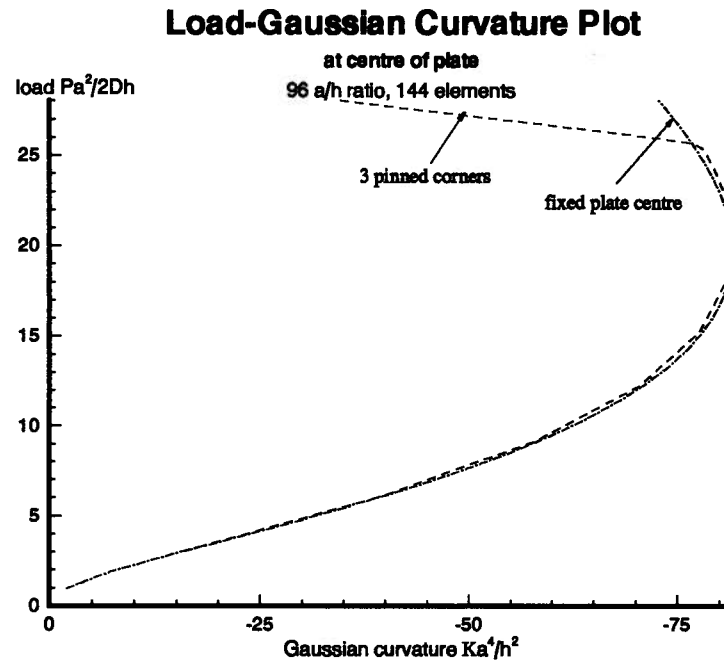


Figure 4.29: Load-Gaussian Curvature Plot for fixed plate centre

stretching the plate. Further study involving “follower forces” which remain normal to the plate surface is recommended to study the effects of the added membrane tension.

4.7 Alternate Finite Element

The finite element analysis was also performed modelling the plate with the SHELL43 4 node shell element. The SHELL43 element is claimed by ANSYS to be well suited to model nonlinear thin to moderately-thick shell structures[8]. The SHELL43 element accommodates rotational degrees of freedom and shear deformations but since the problem under consideration is highly nonlinear, the bilinear SHELL43 element would not be expected to model the plate as well as the quadratic SHELL93 element. The plate modelled with SHELL43 elements did not buckle for the loading case of 3 pinned corners and no initial hydrostatic pressure. The SHELL43 element model only buckled with

Table 4.6: SHELL43 Element Critical Values from Southwell plot

96 a/h ratio, 400 elements			
pressure (Pa)	$\bar{\delta}_o^0$	P_{Scr} (N)	\bar{P}_{Scr}
1	0.00094	did not buckle	
5	0.0047	did not buckle	
10	0.0094	did not buckle	
20	0.018	did not buckle	
30	0.028	295	20.9
40	0.037	292	20.7
50	0.047	285	20.2
100	0.094	285	20.2
500	0.47	225	15.9

Table 4.7: SHELL43 Element Critical Values from Southwell plot

96 a/h ratio, 50 Pa hydrostatic pressure		
elements	P_{Scr} (N)	\bar{P}_{Scr}
16	did not buckle	
64	did not buckle	
144	285	20.2
256	285	20.2
400	285	20.2

an initial deflection greater than 0.3 plate thicknesses (table 4.6) and greater than 144 elements (table 4.7).

For the reasons of problems in buckling, the SHELL43 element was not used in the analysis.

4.8 Non-convergence

The post buckling response for the finite element analysis of the 196.7 a/h ratio plate with 3 pinned corners does not converge. The plate bends to a saddle surface up to

the bifurcation point without numerical difficulties. Shear locking does not seem to be a factor, since increasing the mesh density—decreasing the element a/h ratio—does not rectify the problem.

Chapter 5

Discussions

5.1 FEA Comparison of P_{cr} and $P_{K_{cr}}$

Gaussian curvature at the centre of the plate reaches a maximum absolute value K_{cr} at corner force $P_{K_{cr}}$. The absolute value of K then begins to decrease in magnitude before the bifurcation point P_{cr} (figure 5.1).

Attempting to determine the bifurcation point by a critical Gaussian curvature criterion, such as the Southwell plot method, will underestimate the bifurcation point (figure 5.2).

The critical Gaussian curvature point $P_{K_{cr}}$ is 80 percent of bifurcation point P_{cr} (table 5.1).

The values of K_{cr} and $P_{K_{cr}}$ remain the same for the 3 pinned corners and the fixed plate centre loading cases (figure 4.29). The present work uses corner forces which maintain their original vertical direction parallel to z axis. For large deflections, the orientation

Table 5.1: Comparison of $P_{K_{cr}}$ and P_{cr}

a/h ratio	P_{cr}	$P_{K_{cr}}$	$P_{K_{cr}}/P_{cr}$
49.2	26.9	21.7	0.81
63.2	26.0	20.8	0.80
80.3	25.5	20.3	0.80
96.0	25.1	20.1	0.80
196.7	24.9	19.7	0.79

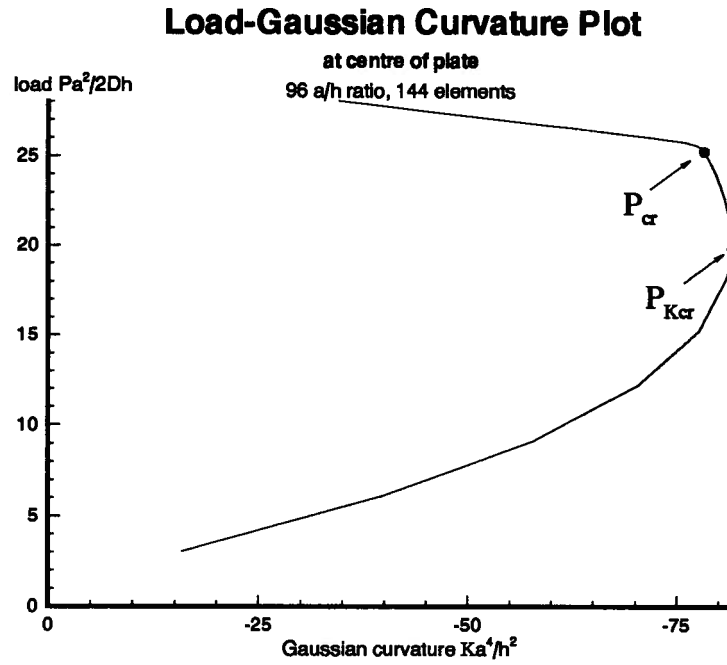


Figure 5.1: Load-Gaussian Curvature Plot

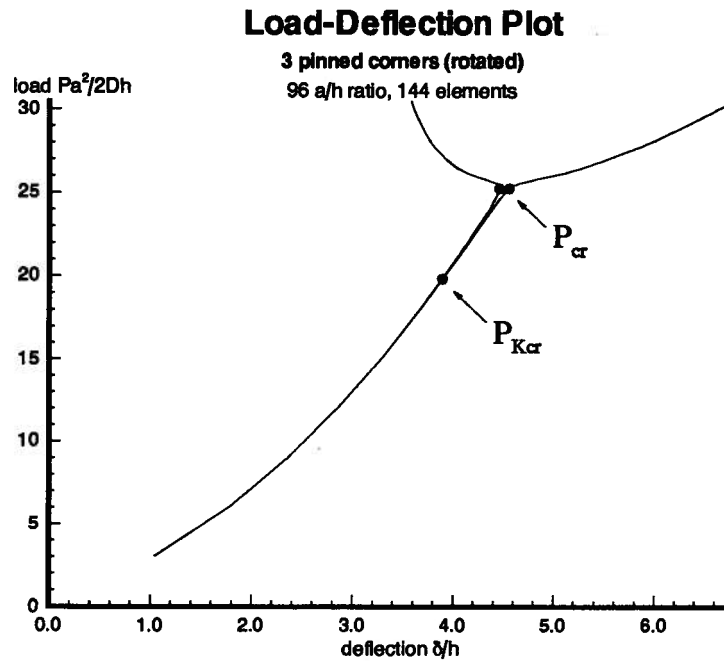


Figure 5.2: Load-Deflection Plot

of the forces causes tensile membrane stresses which may have an effect on the value of P_{Kcr} . Further investigation using “follower forces” which remain normal to the plate surface is recommended.

5.2 Comparisons with Bifurcation Points in Literature

5.2.1 Howell

Howell determined the bifurcation point by experiment[1]. The constraints on the plate in the experiment were three corners pinned and the loaded corner free to deflect with the load applied by a constant direction tensile cable. The 3 pinned corners loading case in the present FEA models this experimental setup. Strain gauges measured strains on the top and bottom surfaces of the plate, and Kirchhoff theory was used to calculate the curvatures from the strains. The critical value of Gaussian curvature at bifurcation was determined using the Southwell plot method.

Howell gives the bifurcation point:

$$\kappa a = 10.8h/a \quad (5.1)$$

for the critical value of twist κ at the centre of the plate.

The present FEA work using the Southwell plot method gives:

$$\kappa a = 9.0h/a \quad (5.2)$$

The difference between the result of Howell and the FEA is mainly due to Howell’s limit of applied corner force. Howell limited the maximum applied corner force P_{max}^{Howell} to avoid plastic yielding of the material. This corresponds to corner loads less than half of P_{Kcr} (table 5.2). The Southwell Plot method only claims accuracy as the load approaches the critical load $P \rightarrow P_{cr}$ (section 2.4).

Table 5.2: Comparison of Coefficient with Howell

a/h ratio	C^{Howell}	C	\bar{P}_{max}^{Howell}	P_{max}^{Howell}/P_{Kcr}
49.2	17.85	9.01	4.8	0.18
80.3	11.07	9.02	10.0	0.39
96.0	10.61	9.03	9.9	0.39
196.7	10.25	9.06	10.9	0.43

Table 5.3: Modified Coefficient

at $\bar{P}_{max}^{Howell} = 9.9$ 96 a/h ratio, 144 elements	
pressure (N)	C'
0.1	8.9
1	9.5
10	10.0
100	9.9
300	9.4
500	8.9

The magnitude of initial deflection affects the Southwell's plot prediction of the critical value. The initial deflection for the experiment of Howell is unknown (figure 5.3).

The Southwell plot method using Gaussian and mean curvatures only up to P_{max}^{Howell} gives modified coefficient C' values closer to Howell's results (table 5.3).

5.2.2 Ramsey

Ramsey determined the bifurcation point by analytical methods[5]. The kinematic results of Green and Naghdi for small deformations superposed on a large deformation of an elastic Cosserat surface, and the restricted form of the general nonlinear theory of shells and plates of Naghdi were used. The critical value of twist κ at bifurcation was determined from a Rayleigh quotient.

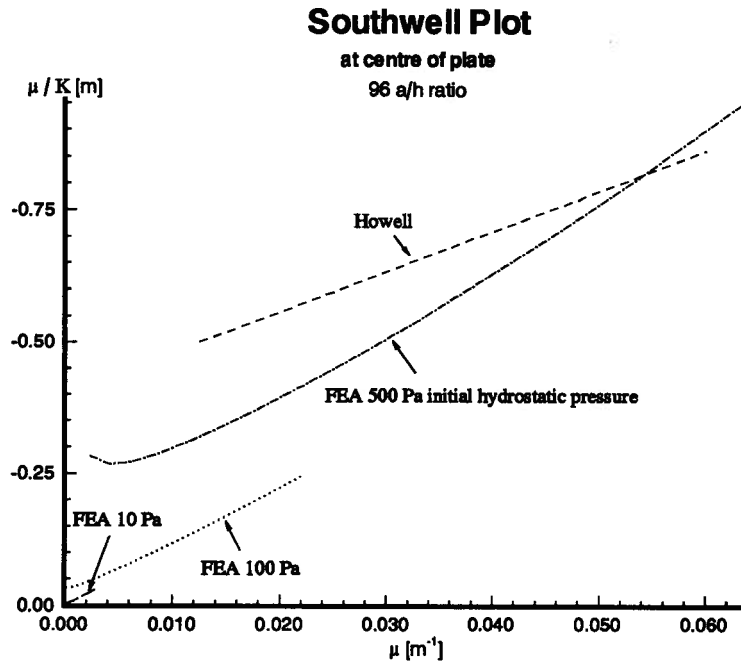


Figure 5.3: Load-Deflection Plot

Ramsey gives the bifurcation point:

$$\kappa a = 3.29h/a \quad (5.3)$$

for the critical value of twist κ at bifurcation at the centre of the plate.

The present FEA work using the Southwell plot method gives results in equation 5.2.

The difference between the result of Ramsey and the FEA is mainly due to Ramsey's assumption of the Gaussian curvature behaviour. Ramsey assumed the Gaussian curvature at bifurcation to be uniform over the plate. The present FEA work shows the Gaussian curvature varies by an order of magnitude over the plate (figure 4.14–4.15).

5.2.3 Miyagawa, Hirata, and Shibuya

Miyagawa, Hirata, and Shibuya determined the bifurcation point by experimental and numerical methods[3].

In the experiment of Miyagawa et al., the critical value of corner force at bifurcation was determined from the load-deflection plot. The plate dimension ratio varied $40 < a/h < 120$. Bifurcation occurred only at ratios $a/h > 80$.

Miyagawa et al. give the bifurcation point experimentally:

$$\bar{P}_{cr} = \left[\frac{Pa^2}{2Dt} \right]_{cr} = 21 \quad (5.4)$$

for the dimensionless corner force \bar{P}_{cr} .

In the numerical work of Miyagawa et al., the deformed configuration of the plate was approximated as a polynomial. Stresses in the middle of the plate were approximated by combining von Kármán theory, an assumed stress function, and experimental results. The relation between load and deflection was determined by minimizing the total energy of: strain energy due to bending and twisting, strain energy in the middle of the plate due to membrane stretching, and work done by the loads.

Miyagawa et al. give the bifurcation point numerically:

$$\bar{P}_{cr} = 22.8 \quad (5.5)$$

The present FEA work using load-deflection plot gives:

$$\bar{P}_{cr} = 25 \quad (5.6)$$

In the experiment of Miyagawa et al., the four loading points were applied by flat roller bearings which simulated “follower loads” to reduce the stretching forces along the plate. The plate material experienced plastic yielding resulting in the experimental bifurcation point of Miyagawa et al. lower than the numerical bifurcation point of Miyagawa et al. [3].

5.2.4 Lee and Hsu

Lee and Hsu determined the bifurcation point by finite difference methods [2]. The critical value of corner force at bifurcation was determined by the displacement-load plot.

Lee and Hsu give the bifurcation point:

$$\bar{M}_{cr} = \left[\frac{(12(1 - \nu^2))^{\frac{1}{2}} a^2}{4(1 - \nu)} \frac{P}{Dh} \right]_{cr} = 21 \quad (5.7)$$

for the dimensionless corner force \bar{M}_{cr} .

The present FEA work using load-deflection plot gives:

$$\bar{M}_{cr} = 61 \quad (5.8)$$

The difference between the result of Lee and Hsu and the FEA is mainly due to the limited model of Lee and Hsu. The mesh used by Lee and Hsu in the finite difference scheme was not dense enough to provide convergence of M_{cr} . No attempt was made to calculate M_{cr} more precisely.

Chapter 6

Conclusions

Describing the surface of a square plate twisted by corner forces based on either displacement or curvature values gives different results for the critical point. The load-displacement plot determines the bifurcation point P_{cr} . The present FEA work gives $\bar{P}_{cr} = 25$. The Southwell plot based on curvature determines the critical Gaussian curvature point $P_{K_{cr}}$. The present FEA work gives $\bar{P}_{K_{cr}} = 20$.

The present FEA work gives the coefficient for the critical value of twist at the centre of the plate $C = 9.0$ from the Southwell plot. This result compares well with the experiment of Howell taking into account the low load levels Howell used to avoid plastic yielding of the material. Southwell plots constructed from curvature data of load levels less than $P_{K_{cr}}$, will overpredict the calculated value of $P_{K_{cr}}$ for initial deflections of the plate centre between $0.001 < \delta_o/h < 0.5$.

The result of the present FEA work does not compare well with the analytical work of Ramsey. Ramsey assumed Gaussian curvature to be uniform over the plate at bifurcation. The present FEA work shows that the problem is highly nonlinear and Gaussian curvature varies over the plate by an order of magnitude at $P_{K_{cr}}$ and P_{cr} .

The applied forces in the present FEA work maintain their original orientation even for large deflections. This will create significant tensile membrane stresses in the plate for deflections much larger than the plate thickness. Further FEA investigation involving "follower forces" which remain normal to the plate surface, and inclusion of nonlinear material properties is recommended.

Bibliography

- [1] R. A. Howell. An experimental investigation of the bifurcation in twisted square plates. Master's thesis, University of British Columbia, 1991.
- [2] S. S. Lee and C. S. Hsu. "Stability of Saddle-like Deformed Configurations of Plate and Shallow Shells". *International Journal of Non-linear Mechanics*, 6:221–236, 1971.
- [3] M. Miyagawa, T. Hirata, and S. Shibuya. "Deformation of Square Plates under Contrary Transverse Load". *Memoirs of Faculty of Technology: Tokyo Metropolitan University*, 25, 1975.
- [4] W. Ramberg and J. A. Miller. "Twisted Square Plate Method and Other Methods for Determining the Shear Stress-Strain Relation of Flat Sheet". *Journal of Research of the National Bureau of Standards*, 50(2):111–123, 1953.
- [5] H. Ramsey. "A Rayleigh Quotient for the Instability of a Rectangular Plate with Free Edges Twisted by Corner Forces". *Journal de Mécanique théorique et appliquée*, 4(2):243–256, 1985.
- [6] R. V. Southwell. "On the Analysis of Experimental Observations in Problems of Elastic Stability". In *Proceedings of the Royal Society*, volume 135 of A, pages 601–616, London, 1935.
- [7] H. H. Spencer and A. C. Walker. "Critique of Southwell Plots with Proposals for Alternative Methods". *Experimental Mechanics*, 15(8):303–310, 1975.
- [8] Swanson Analysis Systems Inc. *ANSYS User's Manual for Revision 5.0*, 1992.
- [9] S. Timoshenko and S. Woinowsky-Krieger. *Theory of Plates and Shells*. McGraw-Hill Book Company, 1959.